IEEE Access
Multidisciplinary ⋮ Rapid Review ⋮ Open Access Journal

Received July 18, 2021, accepted August 1, 2021, date of publication August 17, 2021, date of current version August 27, 2021.

Digital Object Identifier 10.1109/ACCESS.2021.3105609

A Vector Controlled Drive System for Electrically Power Assisted Steering Using Hall-Effect Sensors

RAMY R. SORIAL[1], MOHAMMAD H. SOLIMAN[1], HANY M. HASANIEN[1], (Senior Member, IEEE), AND HOSSAM E. A. TALAAT[2]

[1]Electrical Power and Machines Department, Faculty of Engineering, Ain Shams University, Cairo 11517, Egypt
[2]Electrical Engineering Department, Faculty of Engineering and Technology, Future University in Egypt, Cairo 11835, Egypt

Corresponding author: Hany M. Hasanien (hanyhasanien@ieee.org)

This work was supported in part by the Electrical Engineering Department, Future University in Egypt, Cairo, Egypt, and in part by the Electrical Power and Machines Department, Faculty of Engineering, Ain Shams University, Cairo, Egypt.

ABSTRACT Permanent Magnet Synchronous Motors (PMSMs) have been replacing conventional DC motors in numerous automotive applications. One of which is Electrically Power Assisted Steering Systems (EPAS). PMSMs offer better performance and a longer lifetime while slightly increasing the system's cost and complexity. In a vector-controlled PMSM drive system, the rotor position sensor's resolution plays a vital role in the overall system performance. The better the resolution, the higher the cost. Although numerous sensor-less control algorithms currently exist, machine startup and operation with dynamically changing set-points and loads still impose a challenge for such an approach. For this reason, inexpensive Hall-Effect sensors have been recently used along with a proper position estimation algorithm to provide high-resolution rotor position. In this paper, an implementation of a vector-controlled drive system is applied to an EPAS using only low-resolution Hall-Effect sensors. Additionally, an improved rotor position estimation algorithm based on speed integration is developed to decrease estimation errors and torque ripples in the case of direction reversal. This is to cater to the dynamically changing commands encountered during the normal power assist operation. Comparisons of the proposed rotor position estimation system with the conventional technique are introduced. A complete representation of the proposed system is built using MATLAB/Simulink. An experimental setup is developed and built around a Motor-Driven Power Steering (MDPS) unit which is a column-assist type EPAS system made by Hyundai Mobis. The simulation and experimental results are presented to verify and evaluate the effectiveness of the proposed algorithm.

INDEX TERMS DSP, electrically power-assisted steering, field-oriented control, Hall-effect sensors, PMSM, rotor position estimation.

I. INTRODUCTION

During the past few years, the need for more compact, more efficient, and reliable systems led many automotive manufacturers to head towards replacing conventional direct current (DC) motors with Permanent Magnet Synchronous Machines. This usually comes in exchange for a higher cost. PMSM drives usually require a more complex Electronic Control Unit (ECU) as well as a position sensor mounted on the machine's rotor [1]. Seeking better prices, numerous approaches have been adopted to optimize the system's cost. One of which is the use of sensor-less control algorithms which eliminates the need for a position sensor. Many applications demands can be fulfilled with such an improvement as Fans, pumps, and compressors. Others like EPAS requiring high dynamic performance with dynamically changing set-point and load are hard to be satisfied [2]. Due to their high power density, Surface-Mounted PMSM (SPMSM) is often used in applications with space constraints like the EPAS. Unlike Interior Permanent Magnet Synchronous Motors (IPMSMs), traditional high-frequency injection techniques cannot be used for startup and low-speed operation [3]. This is due to the lack of rotor saliency [4], making it challenging for the system to operate without any physical positional feedback at low and zero speed ranges. Other techniques have been developed to obtain a good balance between cost and performance. One of which is the combination of low-resolution incremental encoders

The associate editor coordinating the review of this manuscript and approving it for publication was Paolo Giangrande.

with low-cost Hall-effect sensors to replace a high-resolution rotary encoder [1]. Other techniques rely on the steering wheel angle sensor combined with a proper sliding-mode observer to estimate an accurate rotor position. Thus, eliminating the need for a dedicated angle sensor for the motor. However, this comes at the cost of more complex mathematical computations [5]. Traditional Brushless DC (BLDC) motors use Hall-effect sensors to measure the rotor position with a resolution of 60 electrical degrees [6]. Although it is possible to use the raw position from the Hall-Effect sensors to drive a PMSM, high current and torque ripple will lead to a noisy and inefficient operation. As a low-cost compromise, these Hall-Effect sensors can be used with a proper algorithm to obtain a high-resolution rotor position. This can be a cost-effective solution offering good dynamic performance and eliminating the need for an initial rotor position estimation algorithm [7]. Some systems use the output speed computed from the Hall-Effect sensors with vector tracking observers that rely on Back-EMF (BEMF) estimation to obtain an accurate position estimate [8]. Seeking a better angle tracking performance over a wide speed and load ranges, non-linear observers can be used together with Phase Locked Loop (PLL) for obtaining an accurate position estimation [9]–[11]. Additionally, other researchers use the spatial Fourier series to interpret the Hall-effect sensor's output as a rotating vector accompanied by a set of harmonics, then feed the resulting angle to a vector tracking observer [12]. The authors in [13] have used fuzzy logic control with the average speed technique to obtain a precise rotor position at low speeds. The purpose of this paper is to present an implementation of an EPAS system powered by an SPMSM. The motor is driven using only low-resolution Hall-effect sensors. An improved rotor position estimation algorithm based on the average speed integration [14] is proposed.

The proposed algorithm uses a Finite State Machine (FSM) to operate the position estimator in three different states: startup, forward estimation, and reverse estimation. During startup, the rotor position is taken from the raw Hall-effect sensor outputs which contain a position error of a maximum of $\pm 30°$ electrical. This tolerable amount of error ensures the correct startup direction of rotation. With the first Hall sensor transition, the estimator switches to the forward estimation state where the position is calculated by numerically integrating the computed speed from the Hall-effect sensors. An incremental number is increased every estimation cycle and multiplied by the computed Hall sensor speed. During deceleration or direction reversal, the estimated rotor position reaches its maximum allowed value at the sector boundary. By then, the estimator switches to reverse estimation. During reverse estimation, the incremental number is gradually decreased every estimation cycle till it reaches zero or the next Hall sensor transition occurs. A simulation of the technique is conducted on MATLAB/SIMULINK. The model contains an EPAS system powered by an SPMSM. An experimental setup is built to challenge the simulation results. The setup uses an ARM Cortex M4 DSP to control a column-assist EPAS unit used in medium-sized passenger vehicles. The unit contains a 6-pole SPMSM with two sets of sensors: a high-resolution incremental encoder and a low-resolution Hall-effect sensor set. The proposed approach tends to have a lower estimation error compared to the traditional average speed technique especially during direction reversal with no impact on the overall system's cost and complexity. It requires lower computational power and is less dependent on the machine parameters when compared to observer-based and PLL-based techniques. Additionally, no initial rotor position estimation algorithm is required during startup.

The paper is organized as follows:

Section 2 contains the detailed model of the system including the mechanical and electrical parts. Section 3 describes the detailed methodology used to estimate high-resolution rotor position information from the Hall-effect sensor. Section 4 contains the simulation results. Section 5 describes the details of the experimental setup as well as the practical results. Section 6 summarizes the conclusions of the work done.

II. SYSTEM MODEL

When the driver manipulates the steering wheel, the torque sensor outputs a signal proportional to the magnitude and direction of the driver's applied torque. The signal is then fed to the Electronic Control Unit (ECU) which then determines the amount of assist torque required. Based on this, the electric motor is engaged.

The basic components of a column-assist EPAS system are: the steering wheel, steering Torque & angle sensor, Assist motor, ECU, and the rack & pinion.

A. MECHANICAL SYSTEM MODEL

While the main concern of this paper is the control of the electrical machine, the mechanical model dictates the form and dynamics of the applied mechanical load.

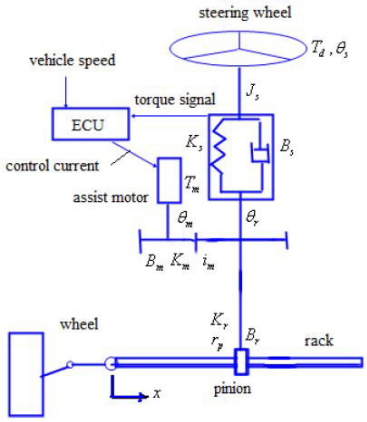

FIGURE 1. Mechanical system model [15].

Fig. 1 shows the relationship between its basic components [15] [16]. Below are the rotary and linear dynamics

equations.

$$J_s\ddot{\theta}_s = T_d - K_s(\theta_s - \theta_r) - B_s\dot{\theta}_s \tag{1}$$

$$J_m\ddot{\theta}_m = T_m - K_m(\theta_m - I_m\theta_r) - B_m\dot{\theta}_m \tag{2}$$

$$m\ddot{x} = \frac{1}{r_p}\left[K_m(\theta_m - I_m\theta_r)I_m + K_s(\theta_s - \theta_r)\right] - B_r\dot{x} - K_r x \tag{3}$$

where $T_d, \theta_s, \theta_r, \theta_m$ and x are the driver's applied torque, steering wheel angle, steering column angle, motor angle, and the rack displacement respectively, J_s and J_m are the steering column and motor inertias respectively, K_s and K_m are the torsional rigidity of the steering column and the coupling between the motor and gearbox respectively, B_s and B_m are the viscous friction coefficients of the steering column and the motor respectively, K_r, B_r *and* M are the steering rack stiffness, viscous friction, and the mass of the rack respectively, r_p is the pinion radius and I_m is the reduction ratio of the gearbox.

B. ELECTRICAL MACHINE MODEL IN THE DQ0 COORDINATES

Assuming symmetrical 3-phase sinusoidal currents, and neglecting the effect of saturation, hysteresis, and magnetic flux leakage, the SPMSM model can be represented by the following equations:

$$\begin{cases} v_d = R_s i_d + L_d\dfrac{di_d}{dt} - \omega_e L_q i_q \\ v_q = R_s i_q + L_q\dfrac{di_q}{dt} + \omega_e(L_d i_d + \varphi_f) \end{cases} \tag{4}$$

$$And\ L_d = L_q = \frac{L_{ab}}{2}\ for\ SPMSM \tag{5}$$

where $\boldsymbol{v_d}$ and $\boldsymbol{v_q}$ are the direct and quadrature supply voltages respectively, $\boldsymbol{L_d}$ *and* $\boldsymbol{L_q}$ are the direct and quadrature inductances, $\boldsymbol{i_d}$ *and* $\boldsymbol{i_q}$ are the direct and quadrature axis currents respectively, $\boldsymbol{R_s}$ *and* $\boldsymbol{\varphi_f}$ are the stator phase resistance and the flux linkage established by the permanent magnets respectively, $\boldsymbol{\omega_e}$ is the electrical angular speed in $\boldsymbol{rad/s}$ and $\boldsymbol{p}$ is the differential operator equivalent to $\frac{d}{dt}$. The electromagnetic torque produced by the machine in the rotor reference frame is as follows:

$$T_e = \frac{3}{2}P\left[\varphi_f i_q\right] \tag{6}$$

where $\boldsymbol{P}$ is the number of pole pairs. The motion equation of the motor is as follows:

$$J_m\frac{d\omega_m}{dt} = T_e - T_L - B_m\omega_m \tag{7}$$

$$And\ \omega_m = \frac{\omega_e}{P} \tag{8}$$

where ω_m is the mechanical rotor angular speed and T_L is the load torque.

III. ROTOR POSITION ESTIMATION USING HALL-EFFECT SENSORS

A. ROTOR ANGLE MEASUREMENT USING HALL-EFFECT SENSORS

Three Hall-Effect sensors facing the rotor poles having an angular spacing of 60 electrical degrees are used as shown in Fig. 2 to measure the rotor position [6].

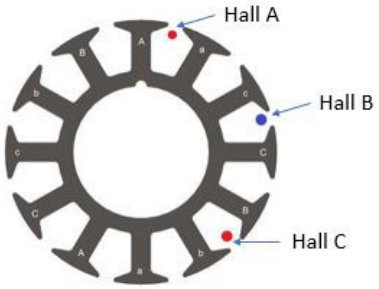

FIGURE 2. Hall effect sensor placement.

The alternation of the rotor poles in front of the sensors while the machine is rotating causes their output state to toggle. For one complete electrical revolution, six distinct sectors and six transitions are produced as shown in Fig. 3 [17].

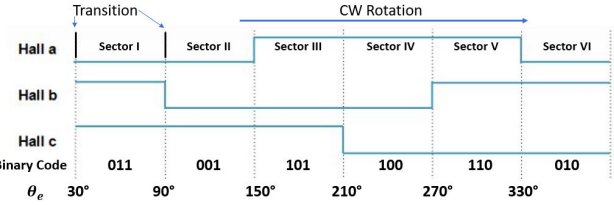

FIGURE 3. Hall-effect sensors output signals.

The combination of the three Hall-Effect sensors output results in a 3-bit binary code. Every time the state of the 3-bit binary code changes, the Hall-effect rotor position is updated indicating a change in the rotor angle. Depending on the current and previous states of this binary code, the rotor position and the direction of rotation can be determined according to Table 1.

The Hall-Effect sensors measured angle illustrated in Fig. 4 compared with the actual electrical rotor angle.

B. ROTOR ANGULAR SPEED CALCULATION

Given that the electrical angle difference between 2 successive transitions is always 60°, it is possible to calculate the rotor angular speed from the hall sensors output by measuring the time duration between 2 successive transitions using the below equation:

$$\omega_h = \frac{\pi/3}{\Delta t} \tag{9}$$

where $\boldsymbol{\omega_h}$ is in rad/s, Δt is the time difference between two successive transitions in seconds.

TABLE 1. Hall sensor position lookup table.

Current State	Previous State	θ_e°	Direction Of rotation	Sector Number
011	010	30	CW	1
	001	90	CCW	
001	011	90	CW	2
	101	150	CCW	
101	001	150	CW	3
	100	210	CCW	
100	101	210	CW	4
	110	270	CCW	
110	100	270	CW	5
	010	330	CCW	
010	110	330	CW	6
	001	30	CCW	

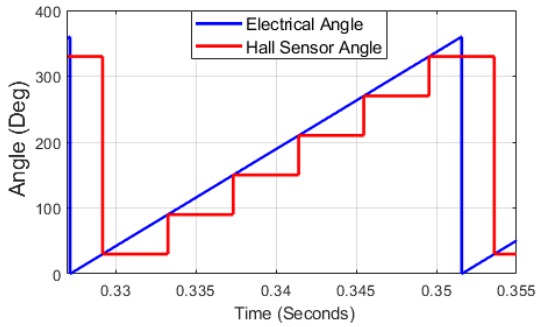

FIGURE 4. Comparison of actual rotor angle to Hall sensor angle.

Although the Hall-Effect sensors measured position can be directly fed to the vector controller to drive the motor, large ripples will appear in the stator currents as well as in the output torque due to the increasing error between the actual rotor electrical angle and the one coming from the Hall sensors. This results in reduced efficiency and noisy operation. The maximum torque ripple can be expressed as a function of the electrical angle error through the following equation [18]:

$$T_r = T_e\left[1 - \cos\left(\tilde{\theta}\right)\right] \tag{10}$$

$$where\ \tilde{\theta} = \theta_h - \theta_e \tag{11}$$

where $\boldsymbol{T_r}$ is the peak-to-peak torque ripple, $\tilde{\boldsymbol{\theta}}$ is the angular error caused by the error in the Hall sensor measurement, $\boldsymbol{\theta_h}$ is the Hall sensor measured angle and θ_e is the actual electrical rotor angle. The maximum angular error $\tilde{\theta}$ happens just before the Hall sensor transition. Fig. 5 shows the electromagnetic torque when the motor is driven using the Hall sensors position only. When the command torque is a 2 *Nm* constant input, the peak-to-peak torque ripple is

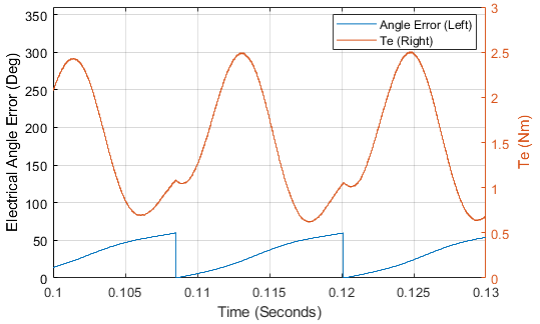

FIGURE 5. Resulting electromagnetic torque ripple when using the Hall-effect sensor measured position.

around 1.85 *Nm*, the rotor's average electrical angular speed is 30 rad/s.

Therefore, an algorithm is required to maintain a low torque ripple, and hence providing a smoother operation with good efficiency.

C. CONVENTIONAL HIGH-RESOLUTION ROTOR POSITION ESTIMATION USING HALL-EFFECT SENSORS

An accurate value of the electrical rotor angle can be estimated by interpolating the values between two hall sensor transitions as a function of the hall sensor angular speed from (9) as follows:

$$\hat{\theta}(t) = \theta_K + \int \omega_h(t)dt \tag{12}$$

where $\hat{\theta}(t)$ is the estimated rotor angle in the time domain and $\omega_h(t)$ is the calculated angular speed from the previous Hall senor transition. The discrete form of the above equation can be written as follows:

$$\hat{\theta}\,(k+1) = \theta_K + \Delta\theta_h \tag{13}$$

$$\Delta\theta_h = \omega_h\,(k)\,nT \tag{14}$$

$$where\ |\Delta\theta_h| < \frac{\pi}{3} \tag{15}$$

where $\hat{\boldsymbol{\theta}}\,(\boldsymbol{k}+\mathbf{1})$ is the next estimated rotor position, $\boldsymbol{n}$ is a number incremented each time the estimation loop is executed, $\boldsymbol{\theta_K}$ $(K = 1, 2, 3 \ldots 6)$ indicates the Hall sensor angle at the current sector and $\boldsymbol{\omega_h}\,(\boldsymbol{k})$ is the calculated Hall sensor angular speed in the previous sector and T is the time interval at which the estimation loop is executed. Every time a transition takes place and the sector changes, the incremental number is reset to zero to align the estimated rotor position with the new sector angle. To prevent large position estimation errors, the estimated angle is saturated around the sector borders as follows:

$$\hat{\theta}\,(k+1) = \begin{cases} \theta_K + \Delta\theta_h, & |\Delta\theta_h| < \dfrac{\pi}{3} \\ \theta_K + \dfrac{\pi}{3} sgn(\omega_h\,(k)), & Otherwise \end{cases} \tag{16}$$

One important case to be studied is during direction reversal. When the machine starts decelerating, the rotor speed decreases. However, since the next Hall sensor transition is

delayed as shown in Fig. 6, the estimated rotor angle $\hat{\theta}(k)$ keeps increasing causing larger estimation errors. It often happens in EPAS systems during maneuvering when the driver abruptly reverses the direction of the applied torque commanding the system to immediately change the direction of rotation.

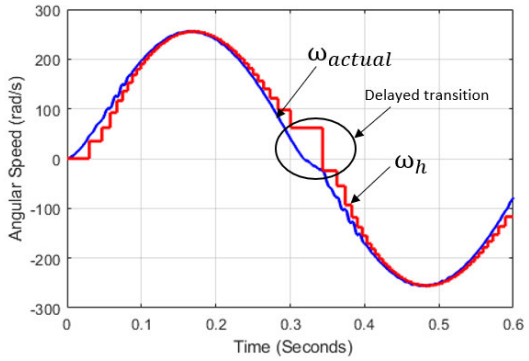

FIGURE 6. Speed estimation error during direction reversal.

High estimated angle errors are causing high ripples in the output electromagnetic torque. Such high ripples, when amplified by the reduction gearbox, will result in an uncomfortable driving experience. Additionally, this might cause some confusion forcing the driver to take unnecessary actions that might compromise the vehicle's safety.

D. PROPOSED ROTOR POSITION ESTIMATION ALGORITHM USING HALL-EFFECT SENSORS

A Finite State sequence is used to control the operation of the estimator, three basic states are implemented to realize the proposed algorithm:

- Startup
- Normal Estimation
- Reverse Estimation

Startup occurs right after the system is powered up. During which, the estimated angle is equal to the left boundary angle of the current sector. This results in a possible initial angle estimation error of 30°.

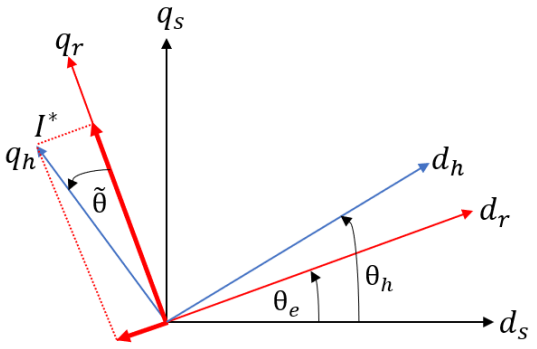

FIGURE 7. Different reference frames during startup.

In Fig. 7, $dr - qr$ denote the actual rotor reference frame while $dh - qh$ denote the imaginary rotor reference frame based on the Hall sensor measurement at startup and has an error of $\tilde{\theta}$. Therefore, I_{dr} *and* I_{qr} can be written as a function of I^* as follows [1]:

$$I_{dr} = -I^* \sin(\tilde{\theta})$$
$$I_{qr} = I^* \cos\left(\tilde{\theta}\right) \tag{17}$$

Substituting in (6) yields:

$$T_e = \frac{3}{2} P \left[\varphi_f I^* \cos(\tilde{\theta})\right] \tag{18}$$

Given a maximum angle error of 30°, the resulting electromagnetic torque will have a value of 86.6% of the actual commanded value in the same direction and hence, the startup is always possible [12].

Once the motor starts spinning, with the first Hall sensor transition, the state is changed to Normal Estimation. During the normal estimation, (13) and (14) are used to evaluate the high-resolution rotor position. Once the condition in (15) becomes false, the state is changed to reverse estimation. During the reverse estimation, the estimator works in the opposite direction by decrementing the count variable n till the next Hall sensor transition occurs or the count variable reaches zero, then it returns to normal estimation. The estimation cycle runs right before the Field-Oriented Control (FOC) loop providing the updated estimated position, which means they are both running at the same rate. Fig. 8 shows the flow chart illustrating the improved estimation technique.

E. SYSTEM BLOCK DIAGRAM

The measured stator currents are compared with the reference direct and quadrature axis currents. The q-axis command is proportional to the driver's input torque determining the amount of required assist while the d-axis current command is set to zero for maximum efficiency. The error signals are then fed to two discrete PI controllers to determine the appropriate output voltages to correct the error, $K_P = 0.02$ and $K_I = 5$ [19]. The motor is driven by a 3-phase Voltage Source Inverter (VSI) powered from a DC source similar to the vehicle DC bus which is 12V. The Hall-Effect sensor outputs are then fed to the speed and angle calculator which uses the data listed in Table 1 to calculate the corresponding angle of the sector number. By differentiating the Hall sensor angle, the rotor speed is obtained accordingly. The rotor position estimator block estimates the electrical rotor angle based on the inputs from the Hall sensor's computed angle and speed. Fig. 9 shows the overall system block diagram of the proposed PMSM drive system using Hall effect sensors. Space Vector Pulse Width Modulation (SVPWM) is used to drive the inverter gates [20].

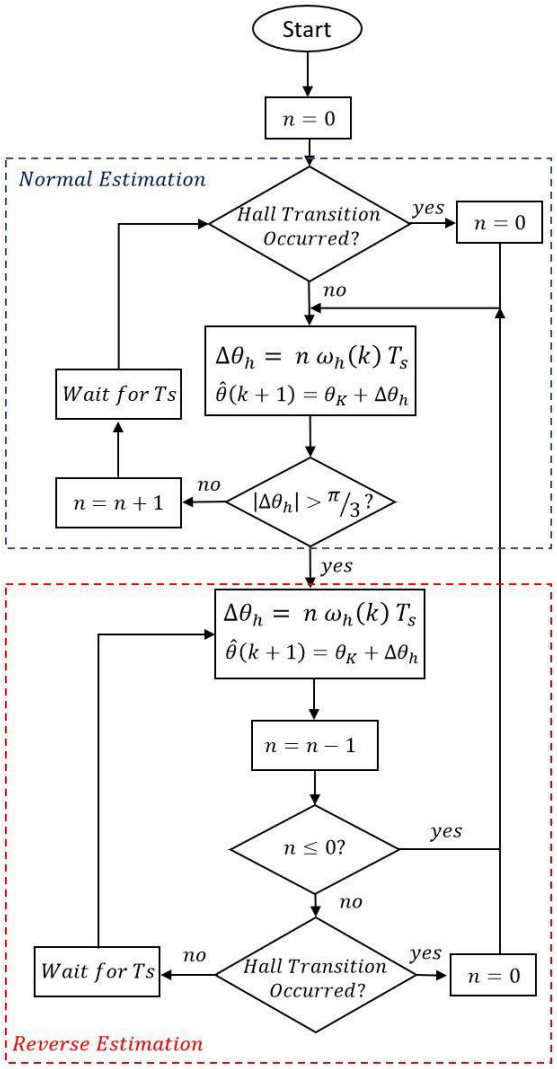

FIGURE 8. Improved position estimation flow-chart.

F. SIMULATION PARAMETERS

Since most modern motor drives use digital controllers, the ECU has been modeled in the discrete-time domain with a sampling time of 100 μs while the electrical machine and the mechanical system were modeled in the continuous-time domain using Sim-Power Systems and Sim-Scape respectively. The PWM frequency for the SVPWM is set to 24 KHz. Table 2 contains the SPMSM parameters used for the simulation [1].

TABLE 2. SPMSM parameters.

Parameter	Symbol	Value
Stator Phase Resistance	Rs	0.023 Ω
Synchronous inductances	Ld, Lq	68 μH
Pole Paris	P	3
PM flux linkage	φ_f	0.0109 V.s

The mechanical system parameters are shown in Table 3. The parameters related to the motor have been obtained from [1] while the remaining parameters have been obtained from [15] except for rp and M which have been experimentally measured using a vernier caliper and weight scale respectively. Im has been calculated by observing the number of turns the input shaft needs to do in order to obtain one full turn at the output shaft.

TABLE 3. Mechanical system parameters.

Parameter	Symbol	Value
Torsion Bar rigidity	Ks	200 Nm/rad
Column Viscous friction	Bs	0.26 Nm/(rad/s)
Column Inertia	Js	0.0012 kg.m^2
Motor Coupling Rigidity	Km	50 Nm/rad
Motor Inertia	Jm	0.00011 kg.m^2
Motor Viscous Friction	Bm	0.00021 Nm/(rad/s)
Gearbox Reduction Ratio	Im	20
Pinion Radius	rp	0.01 m
Mass of Rack	M	5.5 kg
Rack Viscous Friction	Br	653.203N/(m/s)

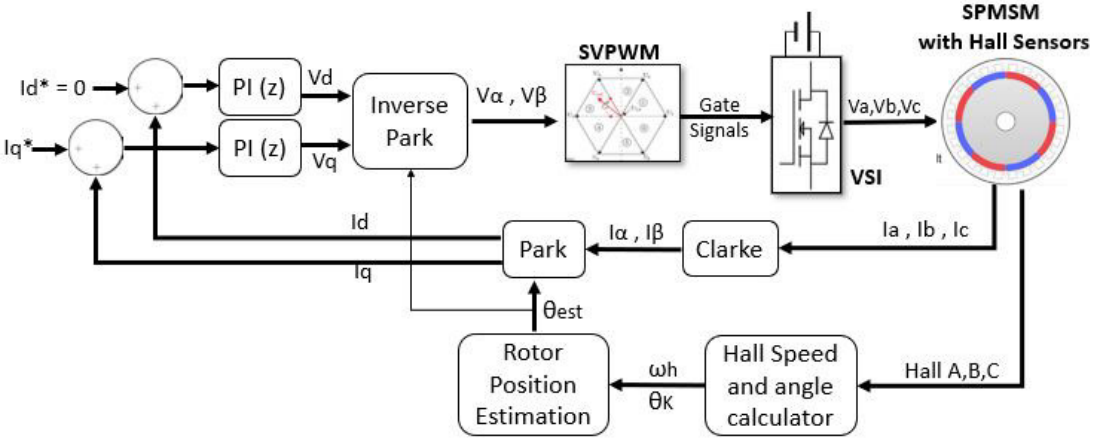

FIGURE 9. Overall system block diagram.

IV. SIMULATION RESULTS

This section evaluates the performance of the improved estimation algorithm through simulation performed using MATLAB/Simulink.

A. SYSTEM RESPONSE TO A CONTINUOUS TORQUE COMMAND

The system is fed with a constant torque command of 1.55 *Nm* equivalent to a q-axis current command of 30*A*.

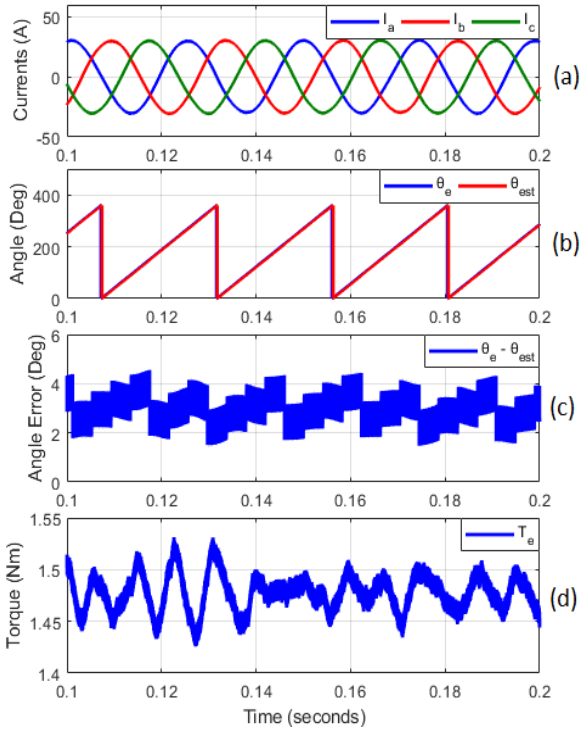

FIGURE 10. Simulated system response to a constant torque command using the conventional angle estimator: (a) stator currents. (b) Rotor angles. (c) Angle estimation error. (d) Electromagnetic torque.

As seen in Fig. 10, the maximum angle error is less than 5° electrical, the peak-to-peak electromagnetic torque ripple is less than 0.1 *Nm*, or 6.45% of the total commanded torque at an electrical angular speed of 257 *rad*/*s*.

With the improved estimator, as shown in Fig. 11 the maximum angular error is also below 5° electrical, the peak-to-peak electromagnetic torque ripple is 0.085 *Nm* or 5.48%.

It can be noted that the proposed system offers a 1% less electromagnetic torque ripple compared with the conventional approach.

B. SYSTEM RESPONSE TO A SINUSOIDAL TORQUE COMMAND

In this section, the system is fed with a sinusoidal torque command with an amplitude of 1.55 *Nm* (equivalent to 30 *A* q-axis current) and a frequency of 10 *rad*/*s*.

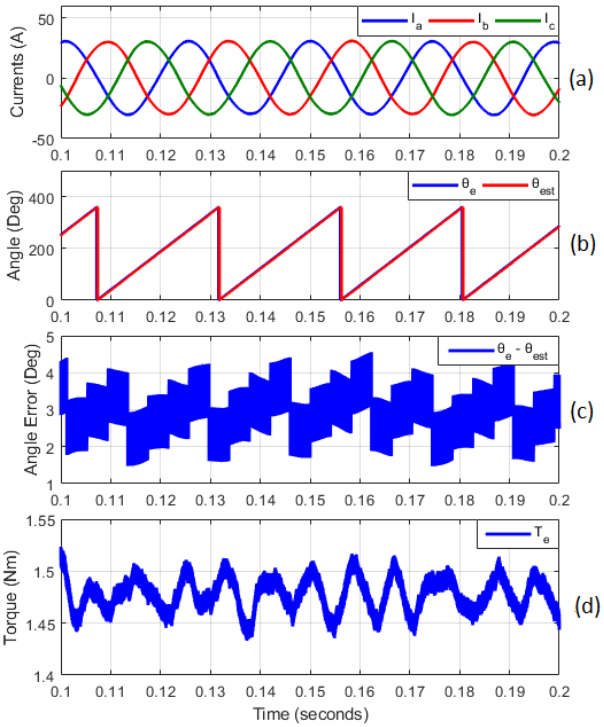

FIGURE 11. Simulated system response to a constant torque command using the improved angle estimator: (a) stator currents. (b) Rotor angles. (c) Angle estimation error. (d) Electromagnetic torque.

1) ESTIMATED ANGLE ERROR

With the proposed technique, the maximum angle error is 42.8° as shown in Fig. 13, compared with 60.45° with the conventional technique, as shown in Fig. 12.

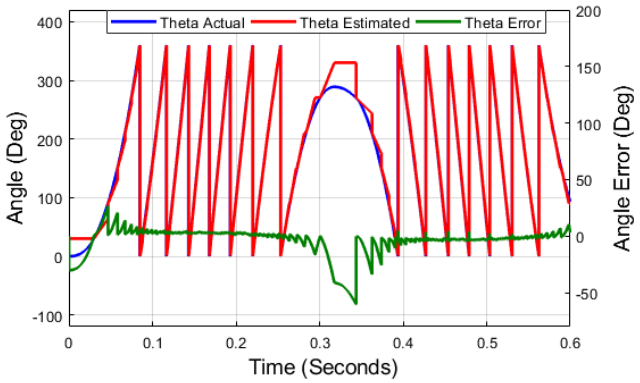

FIGURE 12. Electrical rotor angle error with the conventional technique when the system is subjected to a sinusoidal torque command.

2) ELECTROMAGNETIC TORQUE RIPPLE

With the conventional technique, the peak-to-peak electromagnetic torque ripple is 0.547 *Nm*, or 35.3% of the peak command torque as shown in Fig. 14.

With the improved technique, the peak-to-peak electromagnetic torque ripple is 0.486 *Nm*, or 31.35% of the peak command torque as shown in Fig. 15.

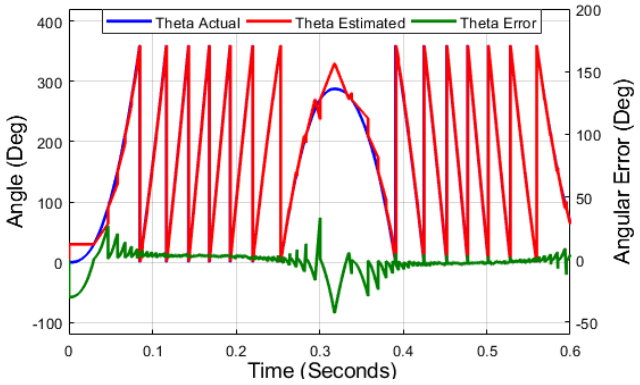

FIGURE 13. Electrical rotor angle error with the proposed technique when the system is subjected to a sinusoidal torque command.

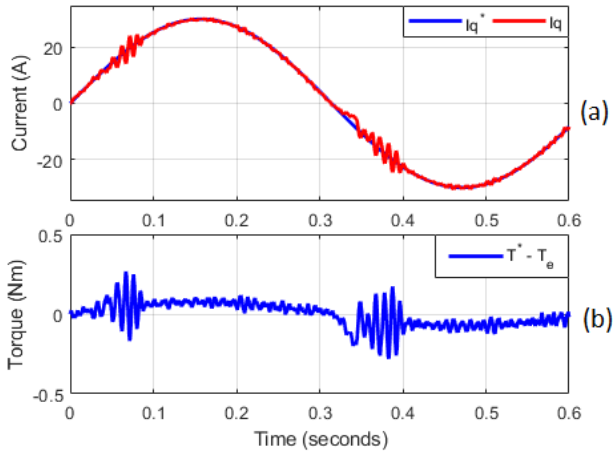

FIGURE 14. Electromagnetic torque ripple with the conventional technique when driven by a sinusoidal torque command: (a) q-axis currents. (b) Electromagnetic torque ripple.

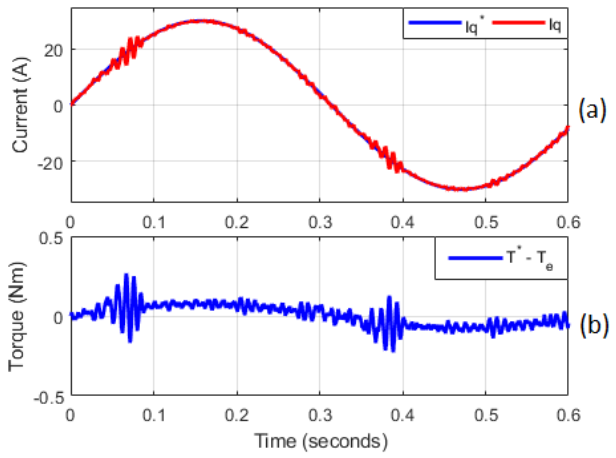

FIGURE 15. Electromagnetic torque ripple with the improved technique when driven by a sinusoidal torque command: (a) q-axis currents. (b) Electromagnetic torque ripple.

The improved technique offers a 4% torque ripple reduction with better command tracking performance.

C. DISCUSSION

Simulation using MATLAB/Simulink has been performed in order to investigate the feasibility of the proposed idea and to study the system's response. As a result, the improved estimator achieved a lower rotor position estimation error when compared with the traditional technique. The latter had the effect of achieving a lower q-axis current ripple which has led to less electromagnetic torque ripple. A comparison between the traditional and proposed techniques is summarized in Table 4.

TABLE 4. Performance comparison between the simulated conventional and improved techniques with a sinusoidal torque command.

Rotor position source	Conventional	Improved
Peak-Peak angle error	60°	42.8°
Peak-Peak torque ripple	0.28 Nm	0.26 Nm
Peak-to-Peak q-axis current error	4.75 A	4.55 A

V. EXPERIMENTAL SETUP AND RESULTS

A. SYSTEM RESPONSE TO A CONTINUOUS TORQUE COMMAND

To verify the performance of the overall system with the proposed improvement, an experimental setup is built around a Motor-Driven Power Steering (MDPS) unit which is a type of column EPAS used in mid-size passenger vehicles. A block diagram of the setup is shown in Fig. 16.

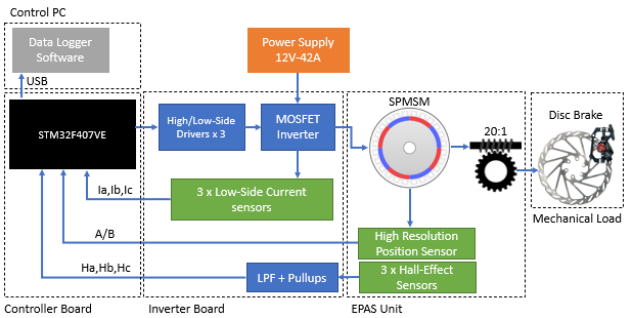

FIGURE 16. Experimental setup block diagram.

1) THE ASSIST MOTOR

The assist motor is a 6-pole SMPMSM with specifications mentioned in Table 2. It contains three hall-effect sensors and an incremental pulse encoder with a resolution of 2048 Pulse per revolution. The sensor board is shown in Fig. 17.

2) THE MECHANICAL SYSTEM

The mechanical system contains a 20:1 worm-type gearbox connecting the motor to the steering column.

A mechanical load is introduced by installing a disc brake system as shown in Fig. 18 simulating the tire-to-ground friction encountered by the EPAS system during normal operation. The amount of applied load is controlled by a brake handle equipped with an adjustment screw to maintain the desired amount of friction.

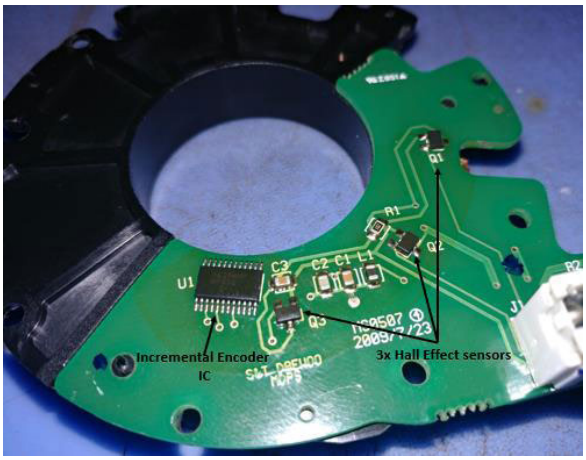

FIGURE 17. Assist motor position sensors board.

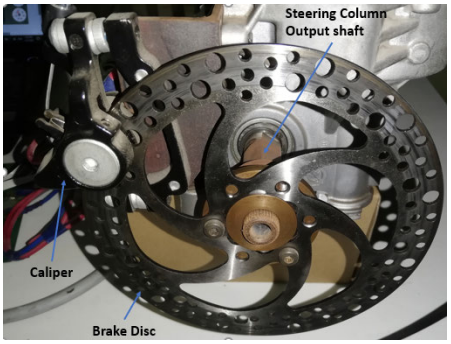

FIGURE 18. Disc brake system.

3) THE ECU

The control algorithms are implemented on an STM32F407 ARM Cortex-M4 based microcontroller kit featuring a Floating-Point Unit (FPU) and running at 168 *Mhz*. The code is written in C and compiled using ARM-GCC on Eclipse IDE and STM32 Cube MX. The torque control is achieved by controlling the d and q-axis currents via two discrete PI controllers $K_P = 0.1$ and $K_I = 3$, the gains have been selected by trial and error. The motor is driven using SVPWM, the PWM frequency is set to 24KHz with a deadtime of 0.595 *us*. Lower PWM frequencies would result in audible noise while higher frequencies would induce more stress on the MOSFET transistors [21]. The FOC control loop is executed every three PWM cycles (125 *us*). The incremental encoder interfaced with the controller using a timer configured in the encoder mode. The three Hall-effect sensor outputs are fed into an input capture module with an XOR input feature which generates an input capture interrupt every time the state of any of the outputs changes [22]. The timer clock frequency is set to 1*MHz*. The raw Hall sensor angle θ_h and direction of rotation are then calculated using Table 1. The rotor angular speed ω_h then calculated using the timer-captured value the below equation:

$$\omega_h = \left(\frac{\frac{\pi}{3}}{ICV}\right) 10^6 \tag{19}$$

where *ICV* is the timer input captured value in micro-seconds and ω_h is in rad/s. The incremental encoder measured rotor position is used as a reference in the assessment of the proposed estimation algorithm (the high-resolution rotor position) with a resolution of 0.527° electrical. Unfortunately, incremental encoders do not report absolute position information. Therefore, at startup, the first Hall sensor transition is used to align the incremental encoder signal to the actual rotor flux position.

A Printed Circuit Board (PCB) was designed and built to interface the various inputs and output to the microcontroller which includes the following:

- A 3-phase MOSFET VSI equipped with three low-side shunt resistors with a value of 750 $\mu\Omega$.
- Three half-bridge MOSFET driver circuits.
- Three fixed-gain low-side current sense amplifiers to measure the stator currents.

To filter out the stator current signals, passive low-pass filters are implemented on the PCB right after the current sense amplifiers as shown in Fig. 19, the cutoff frequency is set to 45*Khz*. Higher frequencies would reduce the filtering effect allowing more noise in the measured current while lower frequencies would cause unnecessary lag in the measurement Furthermore, digital first-order lowpass filters are applied to the d and q-axis current components inside the controller program using the below formula [23]:

$$\begin{bmatrix} i_{df}(k+1) \\ i_{qf}(k+1) \end{bmatrix} = \begin{bmatrix} i_{df}(k) \\ i_{qf}(k) \end{bmatrix} + \frac{2\pi f_c}{f_s} \begin{bmatrix} i_d - i_{df}(k) \\ i_q - i_{qf}(k) \end{bmatrix} \tag{20}$$

where $i_{df}(k+1)$, $i_{qf}(k+1)$ and $i_{df}(k)$, $i_{df}(k)$ are the new and previous filtered d and q-axis currents respectively, i_d , i_d are the unfiltered current values, f_c and f_s are the cutoff and sampling frequency respectively. The cutoff frequency is set to 50 *Hz*. The sampling frequency is 8 *KHz* for a 125 *uS* loop period.

Fig. 20 contains the flowcharts illustrating the various functions performed by the ECU. Due to the timing constraints, most of the time-critical functions are handled by Interrupt Service Routines (ISR). The timer responsible for the PWM generation is also responsible for triggering the Analog-to-Digital converter (ADC) conversions to measure the stator currents. Since low-side current sensors are used, the stator currents are read when the low-side switches are on using the below equation [24].

$$v_{sense} = (i.R_{shunt})A_g + v_{ref} \tag{21}$$

where i is the current flowing into the resistor, v_{sense} is the current sense amplifier output voltage, R_{shunt} is the current sense resistor, A_g is the amplifier's gain which is 50 V/V and v_{ref} is the reference voltage which is set to 1.65 V allowing a full-scale current measurement of ± 44 A per channel.

4) THE COMPUTER SOFTWARE

A program is built using LabView to interface with the ECU for control and data acquisition. The program generates the signal that mimics the driver input torque. It also

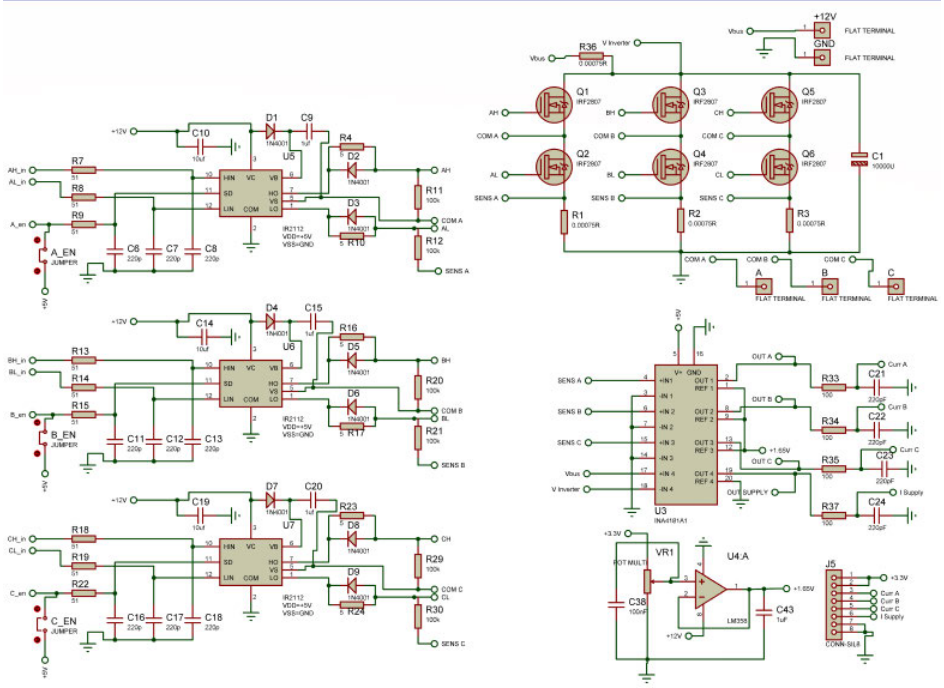

FIGURE 19. Interface PCB schematic.

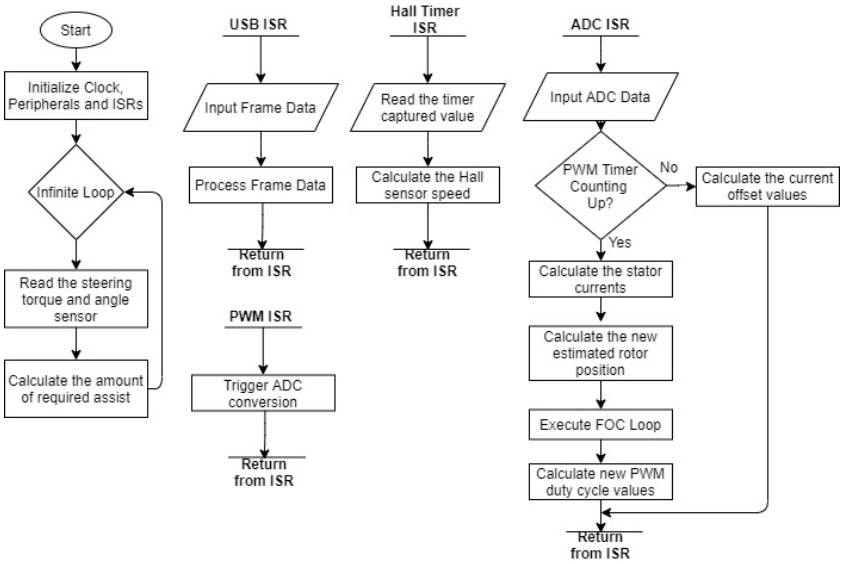

FIGURE 20. ECU program flow chart.

acquires multiple signals from the microcontroller's memory including actual and estimated rotor position, stator currents, and rotor speed. A customized communication protocol is designed for high-speed data acquisition via USB allowing live data to be captured from the ECU at sampling rates reaching 4.5 *Ksps* depending on the data length.

A picture of the complete setup is presented in Fig. 21.

In this setup, the q-axis current command is generated from the PC software.

Two test scenarios were developed to verify the effectiveness of the proposed approach:

- Operation under a constant torque command
- Operation under a sinusoidal torque command

For the purpose of comparison, the rotor position information used with the vector controller is taken from the following sources:

- Raw Hall-effect sensors output
- Traditional Hall-effect sensor position estimator

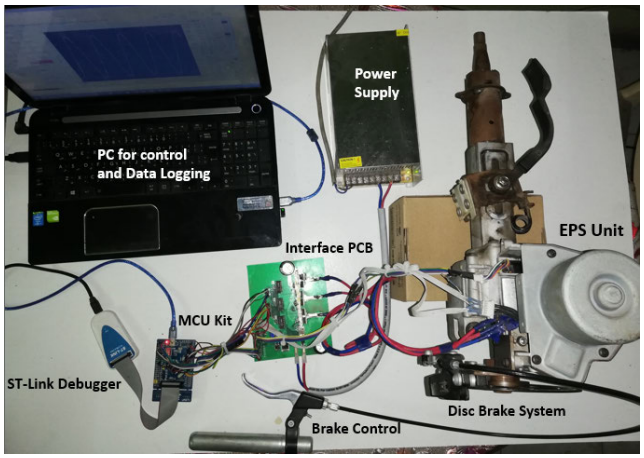

FIGURE 21. Picture of the experimental setup showing various system components.

- Improved Hall-effect sensor position estimator
- High-resolution incremental encoder

The output from the high-resolution rotary encoder is used as a reference to compare the other solutions.

B. SYSTEM RESPONSE TO A CONSTANT TORQUE COMMAND

The system is subjected to a constant torque command equivalent to a 30 *A* q-axis current command (d-axis current command is set to 0).

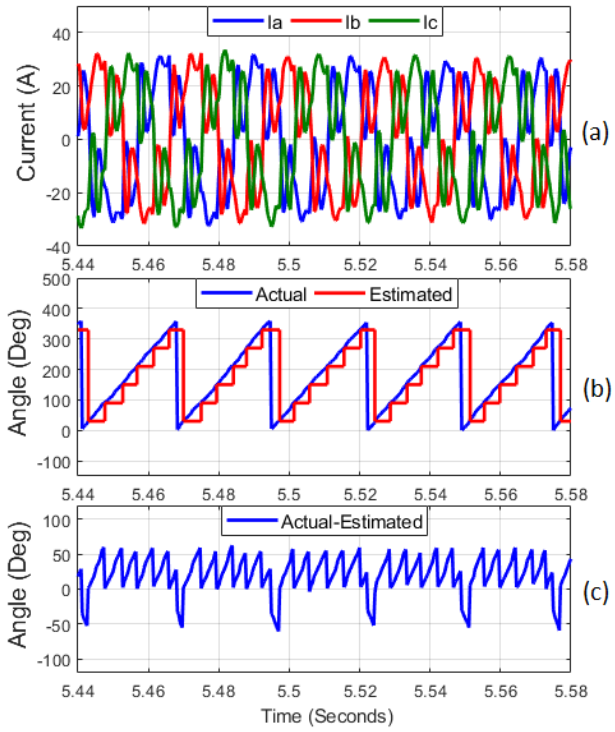

FIGURE 22. Experimental system response to a constant torque command while driven using raw Hall sensors output. a) Stator currents. b) Rotor angles (Actual vs. Hall). c) Angle error.

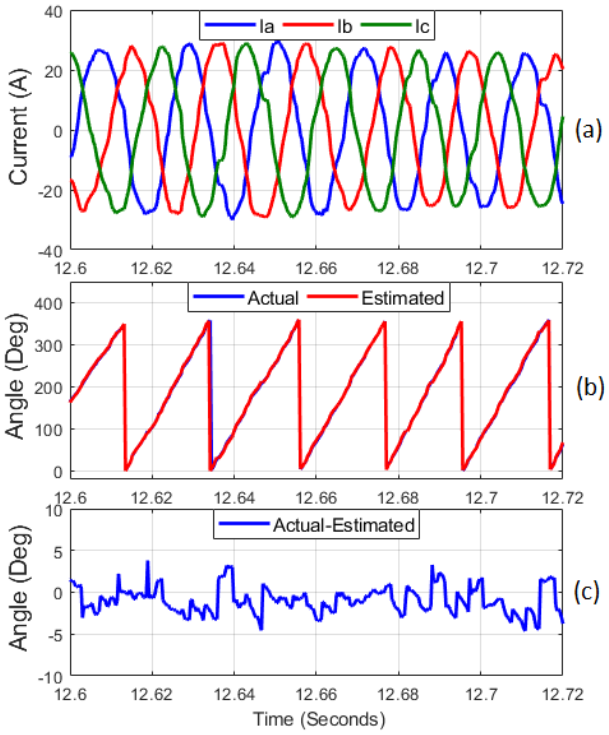

FIGURE 23. Experimental system response to a constant torque command while driven using the conventional hall sensor estimator angle. a) Stator Currents. b) Different rotor angles. c) Angle error.

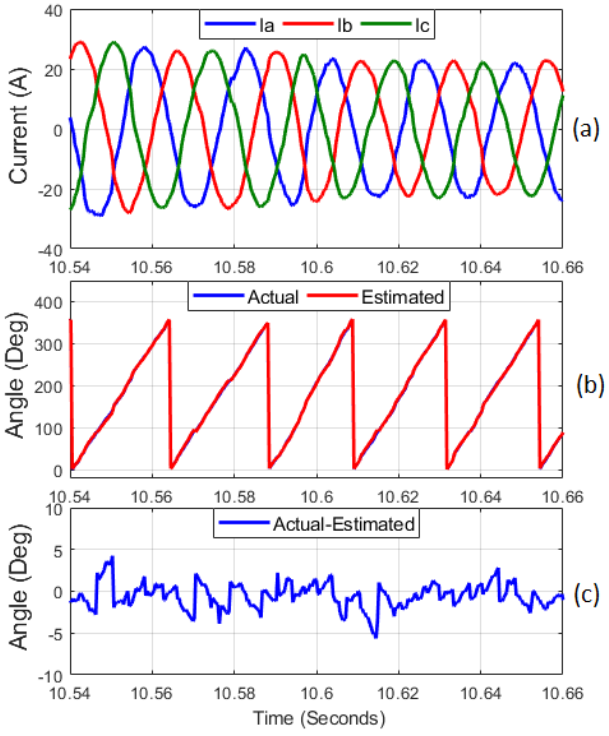

FIGURE 24. Experimental system response to a constant torque command while driven using the improved hall sensor estimator angle. a) Stator currents. b) Different rotor angles. c) Angle error.

Although it is unfavorable, an EPAS system can be operated using only the raw hall sensors output. The maximum angle error will be 60° electrical and the peak q-axis current

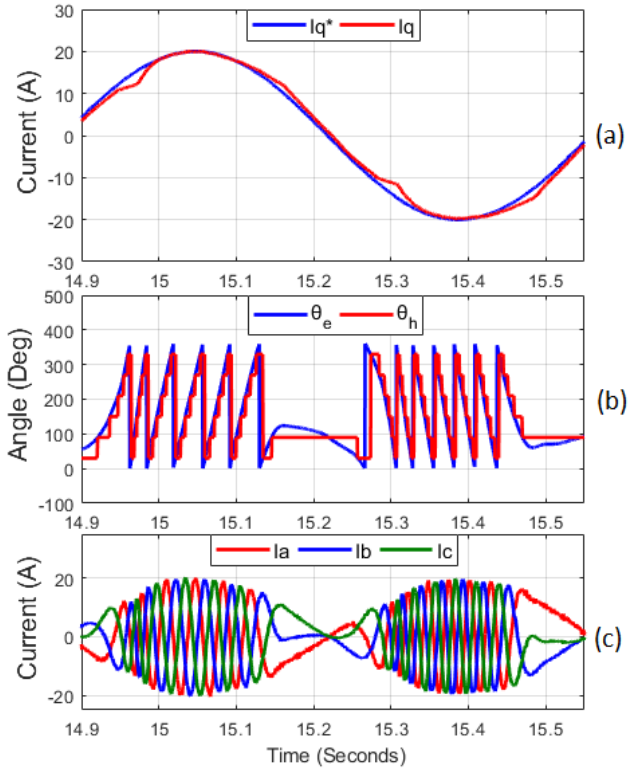

FIGURE 25. Experimental system response to a sinusoidal torque command while driven using the high-resolution encoder angle. a) q-axis command and response. b) Different rotor angles. c) Stator currents.

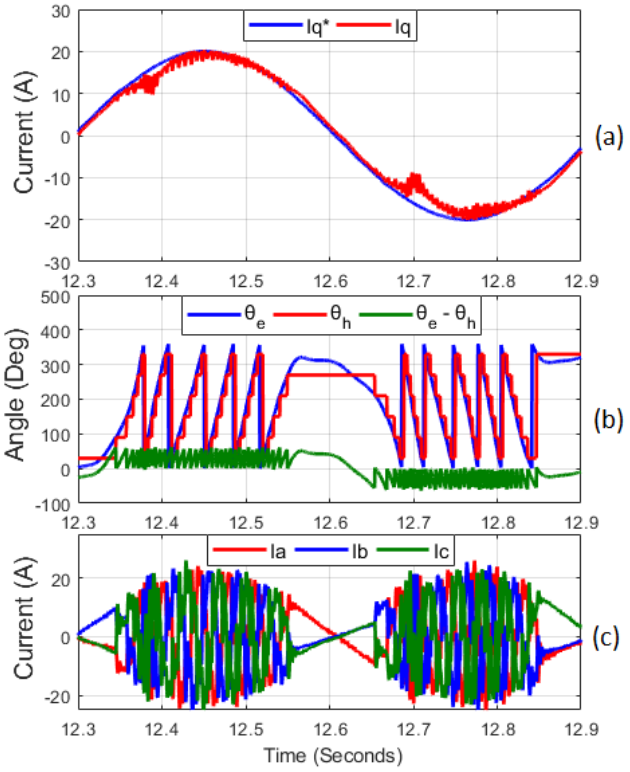

FIGURE 26. Experimental system response to a sinusoidal torque command while driven using the raw Hall-effect sensors angle. a) q-axis command and response. b) Different rotor angles. c) Stator currents.

error ($I_{qref} - I_q$) is **9.4*A*** or **31**% of the current command value.

The downside would be the ripple present in the drive current caused by the varying angular error as shown in Fig. 22. This ripple eventually leads to torque fluctuations which are translated into mechanical vibrations that are amplified by the gearbox affecting the driver's comfort and safety.

Using the hall sensor estimator described using (13)-(16) has the effect of maintaining a maximum angular error of less than 10° electrical as shown in Fig. 23. The difference between the improved estimator technique shown in Fig. 24 and the conventional one is insignificant when the system is subjected to a constant torque command. However, this is not the case in EPAS where the system needs to respond to varying torque commands.

C. SYSTEM RESPONSE TO A SINUSOIDAL TORQUE COMMAND

The system is subjected to a sinusoidal torque command equivalent to 20*A* peak q-axis current command with a frequency of 10 rad/s (d-axis command is set to zero). To achieve the required current command, frictional load torque is applied to the system using the disc brake.

As mentioned earlier, the system's performance when driven using the high-resolution encoder is considered to be the ideal case in this paper since it provides the most accurate rotor position information. This can be seen in Fig. 25 where the stator currents suffer from minimum distortion and the q-axis current command tracking performance is at its best. The peak-to-peak q-axis current error is **6.4** ***A*** or **32**% of the peak command torque. The worst-case scenario is shown in Fig. 26 where the system is driven using the Hall-effect sensor angle. The stator currents are highly distorted, the q-axis current suffers from a high amount of ripple, additionally, audible noise is noticed. The maximum error between the actual angle (the high-resolution encoder) and the hall sensor angle is **60**° while the peak-to-peak q-axis current error is **13.9** ***A*** or **69**% of the peak commanded value.

As shown in Fig. 27, introducing the conventional Hall-sensor angle estimator had the effect of improving the q-axis command tracking performance with lower ripples compared with the previous case. However, the estimator performance significantly drops during direction reversal due to the delayed hall sensor transition. The maximum angle error is **121**° and the peak-to-peak q-axis current error is **8.2** ***A*** or **41**% of the peak commanded value. The stator currents are still slightly distorted due to the sudden jumps in the estimated angle caused by the forced adjustment occurring at each Hall sensor transition [25].

As shown in Fig. 28, by using the improved hall sensor estimator, the stator currents experience much less distortion compared with the previous case while maintaining a good q-axis command tracking performance.

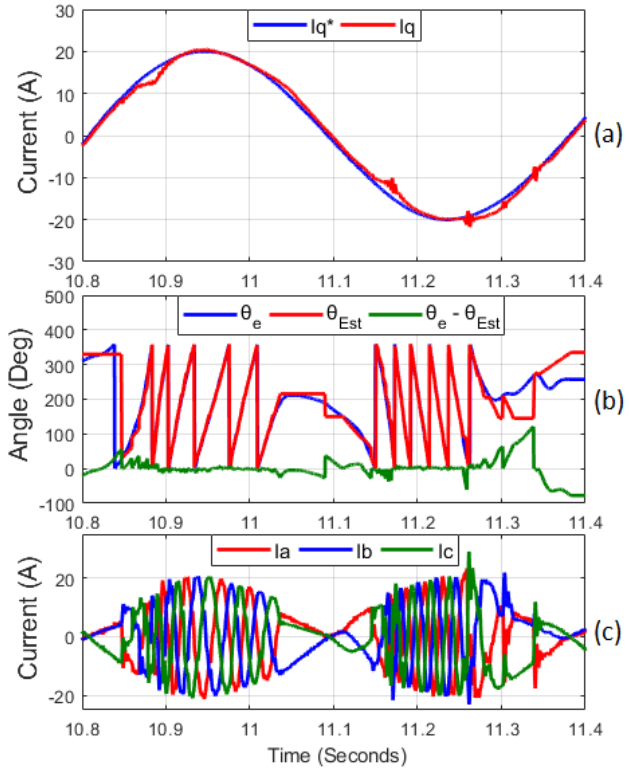

FIGURE 27. Experimental system response to a sinusoidal torque command while driven using the conventional Hall sensor estimator angle. a) q-axis command and response. b) Different rotor angles. c) Stator currents.

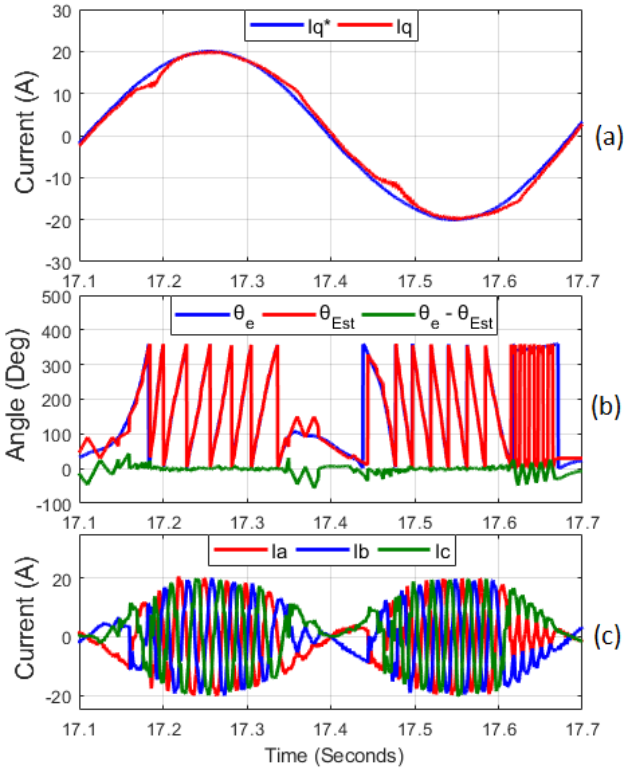

FIGURE 28. Experimental system response to a sinusoidal torque command while driven using the improved Hall sensor estimator angle. a) q-axis command and response. b) Different rotor angles. c) Stator currents.

The maximum estimation error is less than **55**° and the peak-to-peak q-axis current error dops to **7** ***A*** or **35**% of the peak commanded value. Table 5 summarizes the results of the conducted experiment comparing the overall system performance with different rotor position sources.

TABLE 5. Performance comparison between different rotor position estimation techniques.

Rotor position source	High-resolution encoder	Raw Hall Sensor output	Conventional Hall estimator	Improved Hall estimator
Maximum angle Error (Deg)	N/A	60°	120°	55°
Stator Current distortion	Lowest	High	Moderate	Low
peak-to-peak q-axis current ripple	32%	69%	41%	35%

D. DISCUSSION

Experimental verification has been carried out on an actual column-assist EPAS system containing a 6-pole PMSM connected to the steering column via a reduction gearbox. A disc brake system was used to apply frictional load on the steering column simulating the tire-ground friction normally encountered by EPAS systems. As demonstrated in the experimental results section, the proposed algorithm was successfully implemented on the actual hardware. Multiple test scenarios have been considered in order to evaluate the overall system's performance under different conditions when the rotor position information is taken from different sources. The improved technique has shown superior performance compared to the conventional approach.

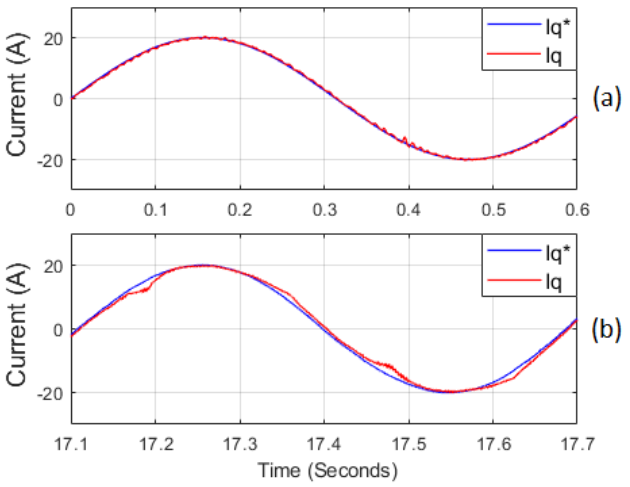

FIGURE 29. System response to a sinusoidal q-axis current command of 10 rad/s and 20 A. while driven using the improved Hall sensor estimator angle. a)Simulation. b) Experimental setup.

A seen in Fig. 29, there exist some differences between simulation and experimental results. These differences are

due to the inverter nonlinearities caused by the deadtime [26], simulated load nonuniformity, and the noise and delay present in the measured stator currents.

VI. CONCLUSION

In this paper, a Vector-controlled PMSM drive has been successfully applied to an Electrically Power-Assisted Steering system using only low-cost Hall-effect sensors. An improved Hall-Sensor angle estimator was implemented to enhance the system's response, especially to a dynamically varying torque command. The latter offered lower estimation error especially in the case of direction reversal. The improved angle estimator offers a maximum angular error of less than 10° electrical when the torque command is constant. When subjected to a sinusoidal torque command, the maximum instantaneous angular error is less than 55° electrical compared to 120° with the conventional method. Although many sensor-less estimation algorithms have been used with vector control, they suffer from sensitivity to parameter variation, require higher computational power, need an accurate estimation for the machine parameters. They require the use of a low-noise current acquisition system. Additionally, for applications requiring a smooth startup, accurate initial rotor position estimation algorithms may be needed. Therefore, the simple technique proposed in this paper would be a favorable choice, offering stable performance less dependent on the machine parameters and load conditions while requiring a minimal amount of computational power similar to that of the traditional average speed technique. Moreover, no initial position estimation algorithm is required since the hall sensors report the initial absolute rotor position information with a tolerable amount of error to ensure a correct startup. In future work, the performance of the system can be further improved by using the positional information from the steering angle sensor mounted on the steering column. The latter can be combined with the technique presented in this paper to obtain a lower estimated angle error, especially in the low-speed region.

REFERENCES

[1] K.-Y. Cho, Y.-K. Lee, H.-S. Mok, H.-W. Kim, B.-H. Jun, and Y.-H. Cho, "Torque ripple reduction of a PM synchronous motor for electric power steering using a low resolution position sensor," *J. Power Electron.*, vol. 10, no. 6, pp. 709–716, Nov. 2010.

[2] Y. Li, H. Wu, X. Xu, X. Sun, and J. Zhao, "Rotor position estimation approaches for sensorless control of permanent magnet traction motor in electric vehicles: A review," *World Electr. Vehicle J.*, vol. 12, no. 1, p. 9, 2021.

[3] P. Kumar, O. Bottesi, S. Calligaro, L. Alberti, and R. Petrella, "Self-adaptive high-frequency injection based sensorless control for interior permanent magnet synchronous motor drives," *Energies*, vol. 12, no. 19, pp. 3645–3670, 2019.

[4] X. Wu, H. Wang, S. Huang, K. Huang, and L. Wang, "Sensorless speed control with initial rotor position estimation for surface mounted permanent magnet synchronous motor drive in electric vehicles," *Energies*, vol. 8, no. 10, pp. 11030–11046, Oct. 2015.

[5] A. Marouf, M. Djemai, C. Sentouh, and P. Pudlo, "Sensorless control of electric power assisted steering system," in *Proc. 20th Medit. Conf. Control Autom. (MED)*, Barcelona, Spain, Jul. 2012, pp. 909–914.

[6] F. G. Capponi, G. De Donato, L. Del Ferraro, O. Honorati, M. C. Harke, and R. D. Lorenz, "AC brushless drive with low-resolution Hall-effect sensors for surface-mounted PM machines," *IEEE Trans. Ind. Appl.*, vol. 42, no. 2, pp. 526–535, Mar. 2006.

[7] Z. Wang, Z. Cao, and Z. He, "Improved fast method of initial rotor position estimation for interior permanent magnet synchronous motor by symmetric pulse voltage injection," *IEEE Access*, vol. 8, pp. 59998–60007, 2020.

[8] S.-Y. Kim, C. Choi, K. Lee, and W. Lee, "An improved rotor position estimation with vector-tracking observer in PMSM drives with low-resolution Hall-effect sensors," *IEEE Trans. Ind. Electron.*, vol. 58, no. 9, pp. 4078–4086, Sep. 2011.

[9] J. Lee, J. Hong, K. Nam, R. Ortega, L. Praly, and A. Astolfi, "Sensorless control of surface-mount permanent-magnet synchronous motors based on a nonlinear observer," *IEEE Trans. Power Electron.*, vol. 25, no. 2, pp. 290–297, Feb. 2010.

[10] V. C. Ilioudis, "PLL type estimator applied in PMSM sensorless control for speed and position," in *Proc. Twelfth Int. Conf. Ecol. Vehicles Renew. Energies (EVER)*, Monte Carlo, Monaco, Apr. 2017, pp. 1–8.

[11] C. Guan-Ren, Y. Shih-Chin, H. Yu-Liang, and L. Kang, "Position and speed estimation of permanent magnet machine sensorless drive at high speed using an improved phase-locked loop," *Energies*, vol. 10, no. 10, pp. 1571–1587, 2017.

[12] Z. M. Dalala, Y. Cho, and J.-S. Lai, "Enhanced vector tracking observer for rotor position estimation for PMSM drives with low resolution Hall-effect position sensors," in *Proc. Int. Electr. Mach. Drives Conf.*, Chicago, IL, USA, May 2013, pp. 484–491.

[13] D. Ban, S. Lee, and J. Hong, "Rotor position estimation of permanent magnet synchronous motors using low-resolution sensors," *Int. J. Fuzzy Syst.*, vol. 19, no. 1, pp. 78–85, Feb. 2017.

[14] Q. Ni, M. Yang, S. A. Odhano, M. Tang, P. Zanchetta, X. Liu, and D. Xu, "A new position and speed estimation scheme for position control of PMSM drives using low-resolution position sensors," *IEEE Trans. Ind. Appl.*, vol. 55, no. 4, pp. 3747–3758, Jul. 2019.

[15] G. Shi, S. Zhao, and J. Min, "Simulation analysis for electric power steering control system based on permanent magnetism synchronization motor," in *Proc. 2nd Int. Conf. Electron. Mech. Eng. Inf. Technol. (EMEIT)*, Shenyang, China, 2012, pp. 1778–1783.

[16] R. R. Hiremath and T. B. Isha, "Modelling and simulation of electric power steering system using permanent magnet synchronous motor," in *Proc. IOP Conf., Mater. Sci. Eng.*, Tamil Nadu, India, 2019, Art. no. 012124.

[17] Y. M. Wang and Q. Fan, "Hall effect sensor based field oriented control of permanent magnet synchronous machine using in electric vehicle," *Adv. Mater. Res.*, vols. 960–961, pp. 1248–1253, Jun. 2014.

[18] R. Ramakrishnan, A. Gebregergis, M. Islam, and T. Sebastian, "Effect of position sensor error on the performance of PMSM drives for low torque ripple applications," in *Proc. Int. Electr. Mach. Drives Conf.*, Chicago, IL, USA, May 2013, pp. 1166–1173.

[19] Mathworks. *Continuous-Time or Discrete-Time PID Controller–Simulink*. Accessed: 2020. [Online]. Available: https://www.mathworks.com/help/simulink/slref/pidcontroller.html

[20] Texas Instruments. (1999). *Space-Vector PWM With TMS320C24x/F24x Using Hardware and Software Determined Switching Patterns*. [Online]. Available: https://www.ti.com/lit/pdf/spra524

[21] R. Krishnan, *Permanent Magnet Synchronous and Brushless DC Motor Drives*. Boca Raton, FL, USA: Taylor & Francis, 2010.

[22] STMicroelectronics. (Feb. 2019). *Reference Manual STM32F405/415, STM32F407/417, STM32F427/437 and STM32F429/439 Advanced Arm-Based 32-Bit MCUs*. [Online]. Available: https://www.st.com/resource/en/reference_manual/dm00031020-stm32f405-415-stm32f407-417-stm32f427-437-and-stm32f429-439-advanced-arm-based-32-bit-mcus-stmicroelectronics.pdf

[23] Microchip Technology. (Mar. 2010). *Sensorless Field Oriented Control of a PMSM*. [Online]. Available: http://ww1.microchip.com/downloads/en/appnotes/01078b.pdf

[24] Texas Instruments. (Mar. 2017). *Current Sensing With <1-µs Settling for 1-, 2-, and 3-Shunt*. [Online]. Available: https://www.ti.com/lit/pdf/TIDUCY7

[25] X. Zhang and W. Zhang, "An improved rotor position estimation in PMSM with low-resolution Hall-effect sensors," in *Proc. 17th Int. Conf. Electr. Mach. Syst. (ICEMS)*, Hangzhou, China, Oct. 2014, pp. 2722–2727.

[26] Q. Guo, Z. Dong, H. Liu, and X. You, "Nonlinear characteristics compensation of inverter for low-voltage delta-connected induction motor," *Energies*, vol. 13, no. 3, p. 590, Jan. 2020.

RAMY R. SORIAL received the B.S. degree in electrical engineering from the Higher Technological Institute (10th of Ramadan City), Egypt, in 2014. He is currently pursuing the M.S. degree in electrical power engineering with Ain Shams University, Cairo, Egypt. In 2014, he joined Ariegsa Manufacturing Group, a company specialized in providing tailored engineering solutions in the field of oil and gas and defense. In 2017, he joined the Technical Research and Development Center, Egyptian Airforces (EAF), participating in different research topics. He is currently leading a Multidisciplinary Team of Engineers, Samaya Electronics Egypt Ltd., (a methode electronics company). The team is responsible for designing, building commissioning, analyzing, and improving manufacturing equipment used in the production of methode's patented magnetoelastic contactless torque and force sensors. The latter is intended to be used in various automotive and e-bike applications. His research is focused on the improvement of electrical drive systems used in automotive applications, developing more efficient, durable, and robust solutions with minimal impact on cost. He is currently focusing on developing cost-effective electrical drive systems to be used in electrically power assisted steering systems, replacing traditional DC motors with the more efficient PMSM. His research interests include developing low-cost protection techniques used in automotive electrical drive systems, improving the overall system's safety, robustness, and fault tolerance.

MOHAMMAD H. SOLIMAN received the B.Sc., M.Sc., and Ph.D. degrees in electrical engineering from Ain Shams University, Cairo, Egypt, in 1999, 2005, and 2011, respectively. He is currently a Staff Member with the Department of Electrical Power and Machines, Ain Shams University. He is a former member of the World Energy Council (2000–2006) and a former Elected Board Member of the Ain Shams University Staff Club (2011–2016). He has been an Elected Board Member with the Electrical Engineering Division, Egyptian Engineers Syndicate, since 2016. He has published several papers in the branch of power electronics applications in power systems, frequency control, voltage control, and electric drives. He has executed and supervised several projects in the field that involved networks design and automation. He won the Prize of the Best Paper in the Youth Symposium at the World Energy Congress, Sydney, Australia, in 2004. He is also a Reviewer for IEEE Access journal.

HANY M. HASANIEN (Senior Member, IEEE) received the B.Sc., M.Sc., and Ph.D. degrees in electrical engineering from the Faculty of Engineering, Ain Shams University, Cairo, Egypt, in 1999, 2004, and 2007, respectively. From 2008 to 2011, he was a Joint Researcher with Kitami Institute of Technology, Kitami, Japan. From 2012 to 2015, he was an Associate Professor with the College of Engineering, King Saud University, Riyadh, Saudi Arabia. He is currently a Professor with the Electrical Power and Machines Department, Faculty of Engineering, Ain Shams University. He has authored, coauthored, and edited three books in the field of electric machines and renewable energy. He has published more than 180 papers in international journals and conferences. His research interests include modern control techniques, power systems dynamics and control, energy storage systems, renewable energy systems, and smart grid. His biography has been included in Marquis Who's Who in the world for its 28 edition, in 2011. He is an Editorial Board Member of *Electric Power Components and Systems Journal*. He was awarded the Encouraging Egypt Award for Engineering Sciences, in 2012, the Institutions Egypt Award for Invention and Innovation of Renewable Energy Systems Development, in 2014, and the Superiority Egypt Award for Engineering Sciences, in 2019. He is currently the IEEE PES Egypt Chapter Chair and the Editor-in-Chief of *Ain Shams Engineering Journal*. He is a Subject Editor of *IET Renewable Power Generation* and *Electronics* (MDPI).

HOSSAM E. A. TALAAT received the B.Sc. (Hons.) and M.Sc. degrees from Ain Shams University, Cairo, Egypt, in 1975 and 1980, respectively, and the Ph.D. degree (Hons.) from the University of Grenoble, France, in 1986. He is currently a Professor of electrical power systems and the Head of Electrical Engineering Department, Future University in Egypt (FUE), Cairo, Egypt. He is on leave from Ain Shams University, Cairo, Egypt. He has authored or coauthored more than 80 technical papers. He has supervised many M.Sc. and Ph.D. theses in the field of power system control and protection. He has taught many undergraduate and graduate courses in this field. His research interests include many research areas, such as application of artificial intelligence techniques (neural networks, knowledge-based systems, genetic algorithms, and fuzzy logic) to power system analysis, control, and protection, real time applications to electrical power systems and machines, and application of optimal and adaptive control techniques for the enhancement of power system stability. He is a member of a number of scientific and technical committees.